PARAMETER OPTIMIZATION AND EXPERIMENT OF AN INSIDE-FILLING PNEUMATIC HIGH-SPEED PRECISION SEED-METERING DEVICE FOR COTTON
/
内充气力式棉花高速精量排种器参数优化与试验

Meng-jie HU*[1,2]; Jia-qi ZHANG[1]; Yao CHEN[1]; Chu-zhen XU[1]; Bao-jia LI[1]
[1]School of Animal Science and Nutritional Engineering, Wuhan Polytechnic University, Wuhan/P.R.China
[2]Key Laboratory of Agricultural Equipment in Mid-Lower Yangtze River, Ministry of Agriculture and Rural Affairs, Wuhan/P.R.China
Tel: +86-027-15527930805; E-mail: humj@whpu.edu.cn
DOI https://doi.org/10.35633/inmateh-76-111

Keywords: *cotton, inside-filling pneumatic high-speed precision seed-metering device, parameter optimization, CFD, DEM-CFD*

ABSTRACT
To address the poor seeding effect of inside-filling pneumatic high-speed precision seed-metering device for cotton, Computational Fluid Dynamics (CFD) and Discrete Element Method–Computational Fluid Dynamics (DEM-CFD) approaches were employed for simulation and optimization. The CFD technique was applied to analyze the influence of key structural parameters of the negative-pressure air chamber on the adsorption performance of the suction holes, while the DEM-CFD approach was used to investigate the motion of cotton seeds inside the seed-metering device during the seed-throwing stage. Based on these analyses, the optimal combination of structural and performance parameters of the seed-metering device was obtained. The simulation-optimized parameters were then validated through bench tests, which showed that at a suction hole diameter of 3.1 mm, a forward speed of 2.33 m/s (8.4 km/h), and a negative pressure of 3,178 Pa, the evaluation indexes were optimal: 96.25% qualification index, 1.83% multiple sowing index, and 1.92% missed sowing index. Further high-speed adaptability test showed that when the forward speed was 1.67~3.33 m/s (6~12 km/h), the qualification index remained greater than 91%, and both the multiple and missed sowing index were less than 5%, meeting the agronomic requirements of high-speed precision seeding for cotton.

摘要
针对内充气力式棉花高速精量排种器排种效果不佳的问题，采用 CFD 和 DEM-CFD 仿真分析方法对其进行了模拟与优化。利用 CFD 仿真分析了负压气室关键结构参数对吸孔吸附性能的影响，采用 DEM-CFD 气固耦合方法探究了投种环节排种器内部棉花种子运动规律，并获得了排种器关键结构与性能参数最佳组合。仿真优化后的参数经台架排种性能试验表明，当吸孔直径为 3.1 mm、前进速度为 2.33 m/s (8.4 km/h)、负压为 3178 Pa 时，其试验指标最优且为合格指数 96.25%，重播指数 1.83%，漏播指数 1.92%。进一步经高速适应性试验表明，当前进速度为 1.67~3.33 m/s (6~12 km/h) 时，合格指数均大于 91%，重播与漏播指数均小于 5%，满足棉花高速精播农艺要求。

INTRODUCTION
Cotton is an important economic crop in China, with a long history of cultivation *(Bie et al., 2018)*. With the acceleration of agricultural modernization, cotton growers are increasingly demanding high-speed and efficient agricultural machinery *(Dong et al., 2025)*. Sowing represents the first step of planting, the seed-metering device being a seeder key component, its seeding quality directly affecting the operational performance of the machine *(Li et al., 2025; Cortez et al., 2020)*. Cotton seed-metering devices are mainly classified into mechanical and pneumatic types. Mechanical seed-metering devices have simple structures but require high seed shape uniformity, having a tendency to damage seeds and suffer from low seeding accuracy under high-speed operation *(Yang et al., 2024; Li et al., 2025; Li et al., 2024)*. In contrast, pneumatic seed-metering devices, although structurally more complex, exhibit better adaptability to seed shape variations, higher seeding precision, and less seed damage, making them more suitable for high-speed seeding operations *(Zang et al., 2024; Li et al., 2021; Gao et al., 2023; Li et al., 2020; Yatskul & Lemiere, 2018; Pareek et al., 2023)*. At present, existing cotton precision seed-metering devices still suffer from poor seed-filling performance under high-speed conditions, with a typical missed sowing index greater than 10%, a qualification index lower than 75%, and the forward speed generally limited to less than 1.11 m/s (4 km/h) *(Zhang et al., 2021; Zhang et al., 2022; Xu, 2018)*.

Since the seed inside-filling type can make use of gravity, centrifugal force, and inter-seed interaction forces to improve the seed-filling performance, our research group previously designed an inside-filling pneumatic cotton high-speed precision seed-metering device. However, experimental results revealed that although the seed-filling performance was improved, the device still exhibited problems such as unstable seed adsorption and poor seed throwing quality under high-speed operation, leading to poor seeding performance. Therefore, the structural parameters of the seed-metering device still require further investigation and optimization.

In recent years, the Computational Fluid Dynamics (CFD) and Discrete Element Method–Computational Fluid Dynamics (DEM-CFD) techniques have been widely applied in the development of seed-metering devices *(Wang et al., 2025; Sun et al., 2025; Wan et al., 2022; Zhou et al., 2024; Guzman et al., 2020; Bustos-Gaytán et al., 2025)*. Guzman validated the feasibility of using DEM-CFD technique to simulate pneumatic seeder planting green field peas through the combination of simulation and experimentation, and investigated the effects of scaled-down seed tank and fluted roller, single run of a horizontal distributor tube, horizontal-vertical tube transition, and vertical seed manifold on the seed movement *(Guzman, 2024)*. Zha et al. designed a branched air-chamber type pneumatic seed-metering device to meet the varying seed rate requirements for different rice varieties, employing CFD technique to optimize the key structural parameters of the branched air chamber casing *(Zha et al., 2024)*. Cao et al. aimed to improve the operational performance of the mixing component in a horizontal air-assisted centralized wheat metering device. Using CFD and DEM-CFD methods, they investigated the influence of key structural parameters of the mixing component on internal airflow distribution and wheat conveying performance, and determined the optimal parameter combination *(Gao et al., 2024)*. Hussain et al. aimed to optimize the working performance of an air-suction maize seed metering device. CFD was used to investigate the effects of vacuum pressure, suction hole diameter, and seed disk speed on device performance, and the optimal parameter combination was obtained. This was subsequently validated through DEM-CFD coupling simulations and bench tests. At a vacuum pressure of 3.5 kPa, an operating speed of 1.94 m/s (7 km/h), and a suction hole diameter of 4 mm, the qualified index reached 95.98%, while the missed index was 1.5% *(Hussain et al., 2025)*. Zhao et al. combined the DEM-CFD gas-solid coupling method and high-speed camera to investigate the effects of key structural and performance parameters of a novel high-speed precision maize seed-metering device on the seeding performance, determining the optimal combination of operating parameters, and verifying the reliability of the seed-metering device under high-speed operation through bench and field tests *(Zhao et al., 2024)*. In summary, simulation techniques are currently widely applied in the development of seed-metering devices for grain crops such as peas, rice, wheat, and maize, while their application in the research and development of high-speed cotton seed-metering devices is not very developed. Moreover, existing studies have not clarified how the air chamber geometry affect the pressure uniformity at suction hole endface for inside-filling pneumatic seed-metering devices, nor have the DEM-CFD coupling simulation been utilized to define the seed throwing pressure and seed throwing port position angle required for stable seed throwing. Therefore, this study uniquely addresses these gaps by combining CFD and DEM-CFD simulations with experimental research to improve the seeding performance of inside-filling pneumatic cotton high-speed precision seed-metering device.

To improve the operational performance of an inside-filling pneumatic high-speed precision cotton seed-metering device, CFD simulations were conducted to analyze the influence of key structural parameters of the negative-pressure air chamber on the pressure at the suction hole end face, and the optimal parameter combination was determined. The DEM-CFD gas–solid coupling technique was then applied to investigate the motion behavior of cotton seeds inside the device during the seed-throwing stage, analyzing the effects of seed-throwing pressure on the initial and stable contact angles between the seeds and the inner wall of the back shell, and determining the optimal seed-throwing pressure and port position. Bench tests of the optimized device were carried out to identify the best combination of performance parameters affecting seeding quality, followed by high-speed adaptability verification. This study provides a reference for the optimization and further improvement of precision seed-metering devices.

MATERIALS AND METHODS

Overall structure and working principle

The inside-filling pneumatic high-speed precision cotton seed-metering device mainly consists of the front shell, seeding plate, suction-hole replacement plate, seed protection board, scraper, seed-cleaning air nozzle, seed-throwing air nozzle, seeding shaft, and back shell, as shown in Fig. 1(a).

As shown in Fig. 1, an arc-shaped groove is arranged on the inner wall of the back shell, which is assembled with the outer wall of the seeding plate to form an air chamber. The back shell is provided with an air outlet hole, which is connected to the air chamber and externally connected to a fan, so that the air chamber can be filled with negative pressure airflow. After cotton seeds enter the inner cavity of the seed-metering device through the seed inlet on the front shell, a seed cluster is formed. The cotton seeds in the lower layer of the seed cluster are adsorbed onto the suction holes under the action of airflow and rotate clockwise with the seeding plate. When the suction hole rotates into the seed cleaning area, excess seeds surrounding the suction hole are removed by the combined action of the scraper and seed cleaning air nozzle, falling back into the seed cluster. The single cotton seed stably adsorbed onto the suction hole is carried by the seeding plate through the seed carrying area and reaches the primary seed throwing area, where it is blown into the collection hole under the action of airflow from the seed throwing air nozzle. As the collection hole continues to move into the secondary seed throwing area, the seed is thrown out through the seed throwing port of back shell, thereby completing the entire seeding process.

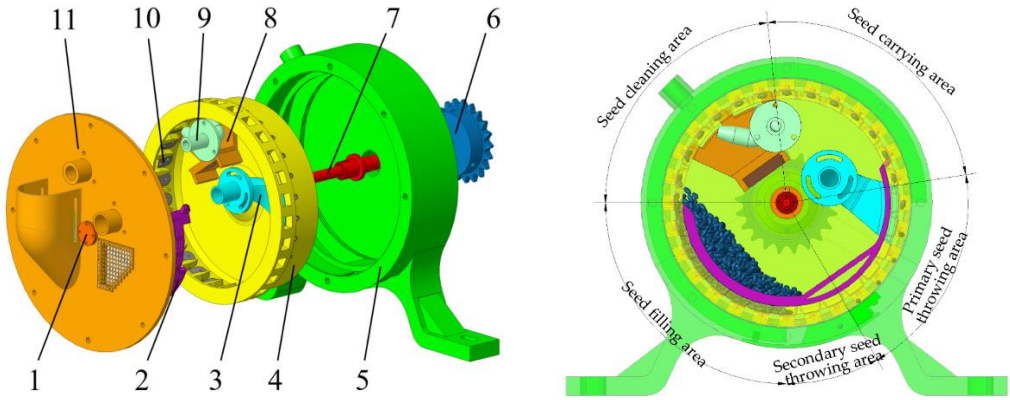

(a) (b)

Fig. 1 - Structural schematic diagram of inside-filling pneumatic cotton high-speed precision seed-metering device

(a) Exploded view diagram of the seed-metering device, (b) Schematic diagram of the working principle of the seed-metering device 1. Bearing end cover; 2. Seed protection board; 3. Seed throwing air nozzle; 4. Seeding plate; 5. Back shell; 6. Sprocket; 7. Seeding shaft; 8. Scraper; 9. Seed cleaning air nozzle; 10. Suction hole replacement plate; 11. Front shell

Simulation analysis method

CFD simulation method for the negative pressure air chamber

Construction and validation of the airflow field model

Using ANSYS Fluent 18.0 software to simulate the airflow field of the negative pressure air chamber, the airflow field model needs to be constructed firstly according to the actual structure and working principle of the seed-metering device, as shown in Fig. 2(a).

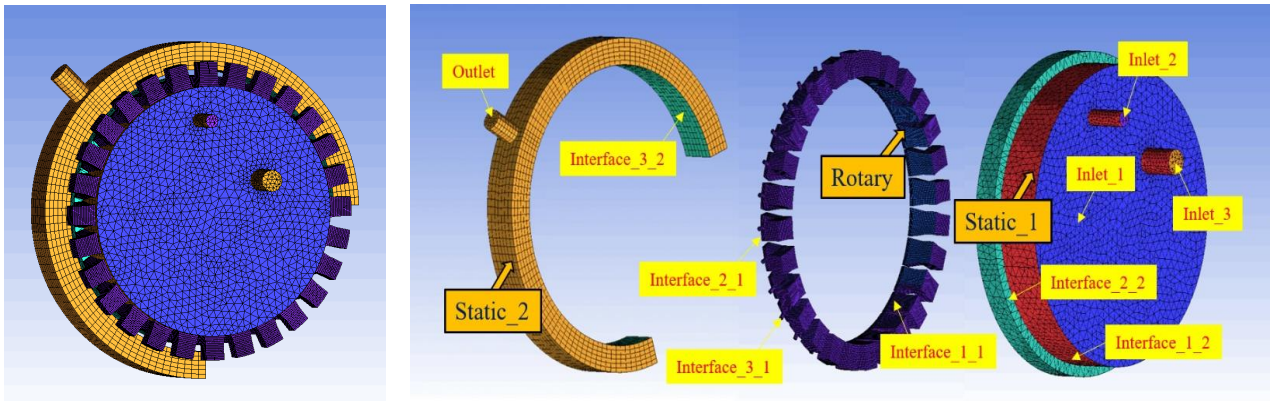

(a) (b)

Fig. 2 - Airflow field mesh model of the seed-metering device

(a) Overall schematic diagram of the mesh model, (b) Exploded schematic diagram of the mesh model

To improve the simulation efficiency, components such as the seeding shaft, seed protection plate, and scraper were omitted to simplify the computational domain. Based on the working principle of the seed-metering device, the airflow field model was divided into one dynamic zone (Rotary) and two static zones (Static_1 and Static_2), as shown in Fig. 2(b). According to the sliding mesh technique, pairs of interfaces were set up between the dynamic and static zones to realize the airflow communication and data exchange across the different regions. Due to the relatively regular geometry of the airflow field in the Rotary and Static_2 zones, structured meshes were applied in these regions. However, the airflow field in the Static_1 zone contains embedded seed cleaning and throwing air nozzles, making it unsuitable for structured meshes, therefore, instead were used unstructured meshes. After meshing the airflow field, the total number of cells was 342356, with the maximum skewness of 0.68. To verify the mesh-independence, two refined meshes with 459749 and 576813 cells were generated for simulation. The pressure differences at the suction hole endface among the three meshes were all less than 5%, indicating that the mesh density had little influence on the pressure at the suction hole endface and that mesh was independent.

In order to test the accuracy of the airflow field model of the seed-metering device, the pressure at the suction hole endface was selected as the evaluation index to carry out the airflow field simulation and physical comparison verification test. Before the test, the central plane of the partition plate between any two adjacent type holes was aligned with the vertical central axis of the seed-metering device, so that the 21 suction holes on the seeding plate were symmetrically and evenly distributed within the negative pressure zone, and sequentially numbered in a clockwise direction, as shown in Fig. 3(a). In the physical test, the pressure at the suction hole endface was measured using a digital differential pressure gauge (Shenzhen Wintact Electronics Co., Ltd., GM520 type, accuracy ±0.3% FSO (factory calibration within 12 months)), and the measurement method was illustrated in Fig. 3(b). The negative pressure at the air outlet was adjusted to –3000 Pa, and after the airflow stabilized, the pressure at suction holes 1–21 was measured and recorded in sequence. The simulation tests were conducted with reference to the physical test, and the boundary conditions were set as follows: the Outlet was set as a pressure outlet with a value of −3000 Pa, the Inlet_1, Inlet_2, and Inlet_3 were set as pressure inlets with the value of 0 Pa, and the rotation speed of dynamic zone was set to 0 r/min. The endface of the suction hole at the measurement points was set as wall. The standard k-ε turbulence model was employed and the pressure-based type solver was selected. The residual convergence criterion was set to 10^{-4}, and the time step was set to 0.003571429, with a total of 500 time steps. After both the physical and simulation tests were completed, the suction holes endface pressure values were compared to verify the accuracy of the airflow field model of the seed-metering device.

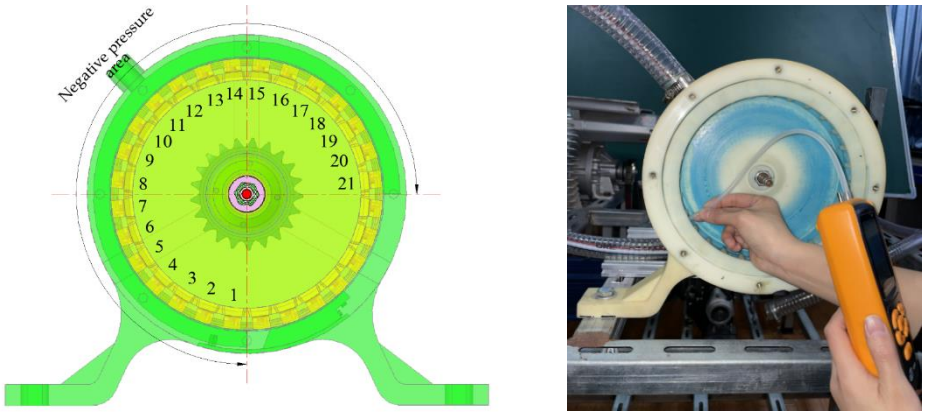

(a) **(b)**

Fig. 3 - Measurement of the pressure at the suction hole endface with the negative pressure setpoint of −3000 Pa

(a) Schematic diagram of suction hole numbering (1~21) in the negative pressure area,
(b) Schematic diagram of physical measurement method
Note: 1. Simulation settings: standard k–ε turbulence model, pressure-based solver, Outlet −3000 Pa, Inlet(s) 0 Pa, dynamic zone rotation speed 0 r/min, residual convergence 10^{-4}, time step 0.003571429 s, 500 steps.
2. Test repeats for 3 times.

Simulation method

The negative pressure air chamber is directly connected to the suction holes, providing the required negative pressure to ensure that cotton seeds remain stably adsorbed on the suction hole endface during the normal operation of the seed metering device. The pressure at the suction hole endface can reflect the adsorption performance of suction hole, and investigating the effects of the structural parameters of the

negative pressure air chamber on the pressure at the suction hole endface can provide a basis for optimizing the parameters of the seed-metering device. The key structural parameters of the negative pressure air chamber mainly include the angle and position of the air outlet hole, and the width and thickness of the negative pressure air chamber.

(1) Effect of Air Outlet Hole Angle and Position on Suction Hole Endface Pressure

The air outlet hole serves as the airflow exit of the seed-metering device, with its angle and position parameters directly affecting airflow direction. These include the position angle, vertical inclination angle, and longitudinal (front–rear) inclination angle, which were therefore selected as test factors to investigate their effect on the pressure at the suction hole endface. Because the suction hole endface pressure is the key factor for stable adsorption of cotton seeds, increasing the endface pressure in the seed-filling area improved the filling performance of the seed-metering device, while reducing pressure variation between suction holes in the seed-cleaning and seed-carrying areas helped prevent missed seeding caused by abrupt pressure changes. Therefore, the average endface pressure in the seed-filling area and the standard deviation of endface pressure in the seed-cleaning and seed-carrying areas were selected as evaluation indexes, and a three-factor, three-level orthogonal test was conducted. The levels of each factor are shown in Table 1, and the angle arrangement was illustrated in Fig. 4. In the numerical simulation, the relevant parameters were set as follows: the Outlet was set as a pressure outlet with a value of −3000 Pa, the Inlet_1, Inlet_2, and Inlet_3 were set as pressure inlets with the value of 0 Pa, and the rotation speed of dynamic zone was set to 30 r/min. The standard k-ε turbulence model was employed and the pressure-based type solver was selected. The residual convergence criterion was set to 10^{-4}, the time step was set to 0.003571429, and the number of time steps was 570.

Table 1

The levels of test factors for orthogonal test

Levels	Test factors		
	Position angle θ_a / (°)	Up and down inclination angle θ_b / (°)	Front and rear inclination angle θ_c / (°)
1	45	-45	-45
2	135	0	0
3	225	45	45

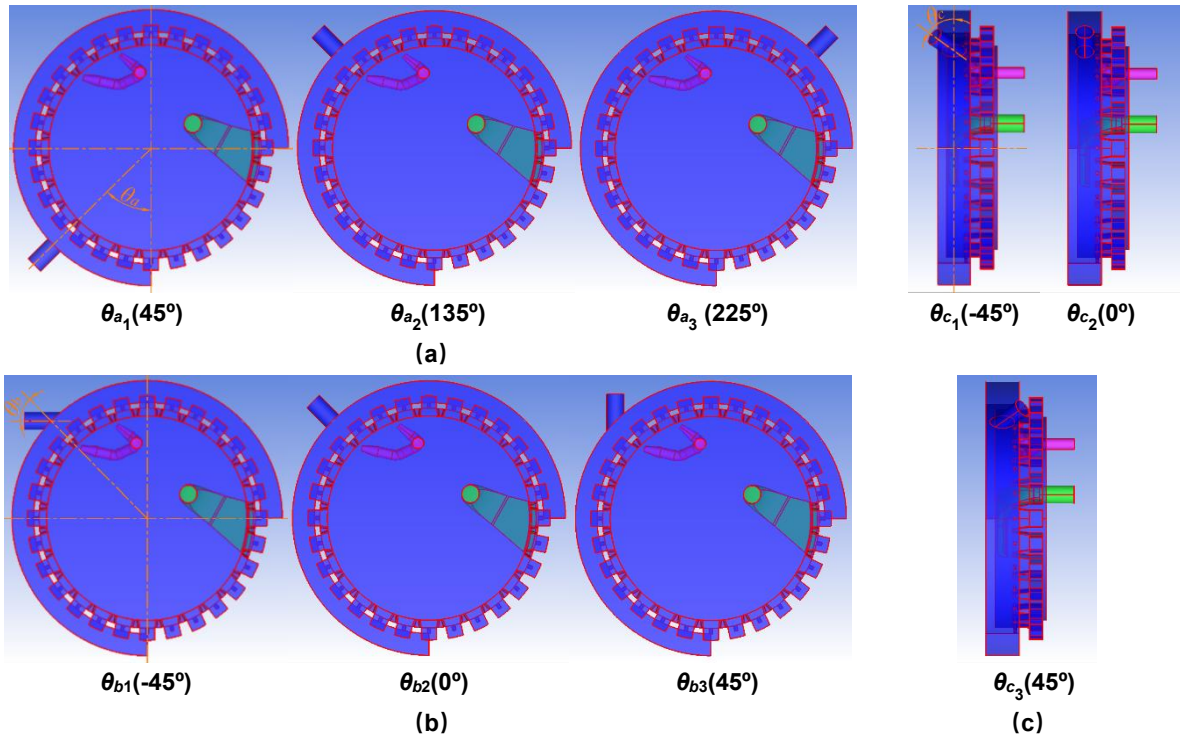

Fig. 4 - Schematic diagram of the angle arrangement of each factor

(a) Position angle, (b) Up and down inclination angle, (c) Front and rear inclination angle

Note: 1. Simulation settings: standard k–ε turbulence model, pressure-based solver, Outlet −3000 Pa, Inlet(s) 0 Pa, dynamic zone rotation speed 30 r/min, residual convergence 10^{-4}, time step 0.003571429 s, 570 steps.

2. Test repeats for 3 times.

(2) Effect of Negative Pressure Air Chamber Width and Thickness on Suction Hole Endface Pressure

The thickness and width of the negative pressure air chamber determine the volume of the air chamber, as shown in Fig. 5, and its influence on the pressure at the suction hole endface can be explored to provide a reference for the optimization of the structural parameters of the seed-metering device. In the simulation test, the air chamber thickness and width were taken as test factors, and the pressure average at the suction hole endface in the seed filling area and pressure standard deviation at the suction hole endface in the seed cleaning and carrying areas were taken as evaluation indexes to carry out a two-factor test.

Based on the actual size of the seed-metering device, the air chamber width b_0 was set at three levels: 22 mm, 26 mm, and 30 mm, while the thickness c_0 was set at 12 mm, 16 mm, and 20 mm. In the flow field model, the position angle, up and down inclination angle, and front and rear inclination angle of the air outlet hole were all set to the optimal levels determined in the previous experiments. All relevant parameters in the Fluent software were kept consistent with the above orthogonal test.

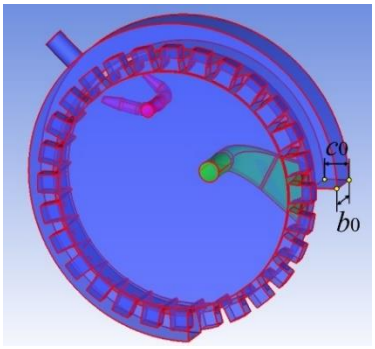

Fig. 5 - Schematic diagram of the width and thickness of the negative pressure air chamber

Note: 1. Simulation settings: standard k–ε turbulence model, pressure-based solver, Outlet −3000 Pa, Inlet(s) 0 Pa, dynamic zone rotation speed 30 r/min, residual convergence 10^{-4}, time step 0.003571429 s, 570 steps. 2. Test repeats for 3 times.

DEM-CFD simulation method for the seed throwing link

In the primary seed throwing area, the cotton seeds adsorbed on the suction hole endface are blown from the filling hole into the collection holes under the airflow action from the seed throwing air nozzle outlet, and then rotated with the seeding plate to the secondary seed throwing area, and finally thrown out through the seed throwing port. The seed throwing air nozzle pressure determines whether cotton seeds can be smoothly blown into the collection hole. To reduce the required air pressure, the seed throwing air nozzle pressure should be selected as low as possible while ensuring the normal operation of the seed-metering device. After cotton seeds fall from the filling hole into the collection hole, collisions between them may cause a certain degree of bouncing. To avoid the impact of bouncing on the seeding performance of seed-metering device, the starting position angle (the angle between the plane formed by the starting edge of the seed throwing port and the center axis of the seeding plate, and the vertical center plane of the seeding plate) of the seed throwing port should be determined to ensure that the seeds have no significant bouncing against the inner wall of the back shell before seed throwing. Since the seeding plate is made of opaque toughness photosensitive resin, and the cotton seeds are coated, the external seed coating agent is easy to adhere to its contact and interfere with the line of sight, so it is not feasible to directly observe the movement of the seeds in the seed throwing area. Therefore, the DEM-CFD gas-solid coupling simulation test method was adopted.

Construction and validation of the cotton seed particle model

EDEM 2018 and ANSYS Fluent 18.0 software were used to perform DEM-CFD gas–solid coupling simulations of the seed-metering device. Bonded particle model (BPM) was adopted to construct cotton seed particles, meaning a single cotton seed consists of several independent fraction particles bonded together. The contact model between fraction particles was set as Hertz-Mindlin with bonding model, and a particle radius of 0.45 mm was chosen. In this study, the E`kangmian-10 cotton seeds (moisture content 11.06% wb, mass of 1000 cotton seeds 94.50 g, length 9.27±0.67 mm, width 5.14±0.37 mm, and thickness 4.50±0.33 mm) were selected as the test material, which can be divided into two categories of ellipsoidal and flat cotton seeds, with the quantity ratio of 22:3, the simulation model being shown in Fig. 6. The ellipsoidal and flat cotton seeds were composed of 146 and 127 fraction particles, respectively. The key components of the seed-metering device were all generated by 3D printing technology with resin materials. Among them, the front shell and seed protection board were made of fully transparent photosensitive resin, while the remaining parts were made of tough photosensitive resin.

Based on previous research and preliminary experiments, the intrinsic material parameters, contact parameters, and main computational parameters used in the coupling simulation are listed in Table 2 *(Hu et al., 2022)*.

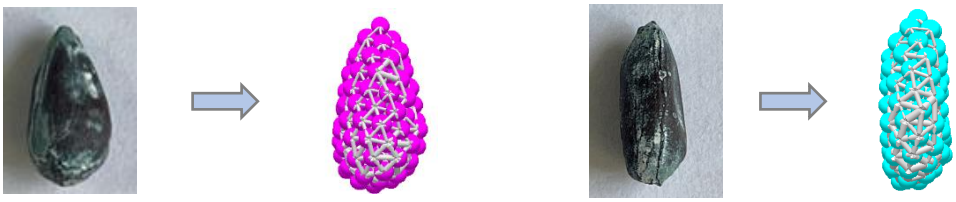

(a) (b)

Fig. 6 - The physical and simulation particle models of cotton seeds

(a) Ellipsoidal cotton seed, (b) Flat cotton seed

Table 2

DEM-CFD coupling simulation parameters

Program	Parameter	Value
cotton seed	Poisson's ratio	0.14
	Shear modulus/(Pa)	4.01
	Density/(kg/m^3)	917
Tough photosensitive resin	Poisson's ratio	0.42
	Shear modulus/(Pa)	1.04×10^9
	Density/(kg/m^3)	1140
Fully transparent photosensitive resin	Poisson's ratio	0.41
	Shear modulus/(Pa)	9.49×10^8
	Density/(kg/m^3)	1268
cotton seed - cotton seed	Restitution coefficient	0.06
	Static friction coefficient	0.10
	Dynamic friction coefficient	0
cotton seed - Tough photosensitive resin	Restitution coefficient	0.13
	Static friction coefficient	0.33
	Dynamic friction coefficient	0
cotton seed - Fully transparent photosensitive resin	Restitution coefficient	0.12
	Static friction coefficient	0.29
	Dynamic friction coefficient	0
EDEM	Solid time step/(s)	3×10^{-7}
	Gravity acceleration/(m/s^2))	9.81
CFD	Fluid	Air
	Density/(kg/m^3)	1.23
	Fluid time step/(s)	3×10^{-5}

Simulation method

Since the number of particles significantly affects the coupling simulation speed, one ellipsoidal and flat cotton seed was used in the DEM-CFD simulation for calculation, respectively. The seed-throwing pressure was selected as the test factor and set at four levels (500, 1000, 1500, and 2000 Pa) based on pre-tests. The initial contact angle—defined as the angle between the vertical center plane of the seeding plate and the vertical line connecting the center of the bonded particle closest to the vertical center plane with the centerline of the seeding plate at the moment the cotton seed first contacts the inner wall of the back shell—and the stable contact angle—measured when the seed shows no significant rebound after contact—were chosen as evaluation indices. These parameters were then used to conduct the coupling simulation test. Since a higher seeding plate rotational speed reduces the time during which the cotton seed is exposed to the airflow from the seed throwing air nozzle in the primary seed throwing area, making it more difficult for the seed to be smoothly blown into the collection hole, the rotational speed of the seeding plate was set to 35.71 r/min (corresponding to the designed maximum forward speed of 3.33 m/s (12 km/h)) to ensure the normal operation of the seed-metering device.

The remaining parameters were set as follows: the Inlet_1 and Inlet_2 were set as pressure inlets with the value of 0 Pa, the Outlet was set as pressure outlet with the value of -3000 Pa. The number of time steps was 100,000 and the simulation time was 3 s. The structural parameters of the negative pressure air chamber were set to the optimal combinations determined from the previous airflow field simulation tests.

The DEM-CFD coupling frequency was set to 3×10^{-5} s, the turbulence–particle coupling was set to two-way data transfer, and the Freestream model was adopted as the drag model. Each cotton seed type was simulated 10 times, the mean was used as the evaluation index, and the minimum value was used as the diagnostic indicator.

Seeding performance test method of the seed-metering device

To investigate the working effect of the simulation-optimized seed-metering device under high-speed operation, the seeding performance tests were conducted.

Test equipment

The test equipment consisted of a self-built performance test platform for the seed-metering device. The main components of the device were fabricated by 3D printing and installed on the platform, as shown in Fig. 7. The seed-metering device was driven by a DC motor through a speed reducer. The detection system employed a self-developed seed-metering device performance testing device for medium and large seeds, which mainly consisted of an LED photoelectric sensing system and a pulse recognition monitoring system, enabling real time monitoring and display of the seeding operation status *(Liu et al., 2021)*.

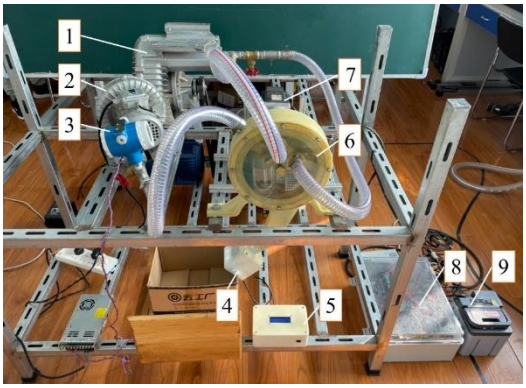

Fig. 7 - Seed-metering device performance test platform

1. Fan Ⅰ; 2. Fan Ⅱ; 3. Pressure gauge; 4. LED photoelectric sensing system; 5. Pulse recognition monitoring system; 6. Seed-metering device; 7. DC motor; 8. Control system; 9. Lithium battery

Test method and evaluation indexes

Referring to GB/T 6973-2005 “Testing Methods of Single Seed Drills (Precision Drills)”, the seed-metering device performance testing device for medium and large seeds continuously detected and recorded the seeding time intervals under stable operation conditions. Every 251 seeds constituted one test group, and each group was repeated 3 times. The qualification index A_1, multiple sowing index D_1 and missed sowing index M_1 were taken as the evaluation indexes, and their calculation formulas were as follows:

$$\begin{cases} A_1 = \dfrac{n_1}{N}\times 100\% \\ D_1 = \dfrac{n_2}{N}\times 100\% \\ M_1 = \dfrac{n_3}{N}\times 100\% \end{cases} \quad (1)$$

where: n_1 is the number of seedings with the seeding time interval between 0.5 and 1.5 times the theoretical value; n_2 is the number of seedings with the seeding time interval less than 0.5 times the theoretical value; n_3 is the number of seedings with the seeding time interval greater than 1.5 times the theoretical value; N is the total number of seedings.

The experimental environmental conditions were a temperature of 25±2℃ and a relative humidity of 50±5%. All experimental runs were randomized.

Test design

Based on previous studies and pre-test, the main factors affecting the seeding performance of the seed-metering device are suction hole diameter, forward speed, and negative pressure. Among them, the conversion formula between forward speed and seeding plate rotational speed was as follows:

$$V_m = \frac{nKI_z}{60} \quad (2)$$

where: V_m is the forward speed, m/s; n is the rotational speed of seeding plate, r/min; K is the number of suction holes, value 28; I_z is the theoretical seed spacing, value 0.2 m.

Therefore, the above three factors were selected as test factors, and the qualification index A_1, multiple sowing index D_1, and missed sowing index M_1 were used as evaluation indexes to conduct the seeding performance tests of the seed-metering device.

(1) A Box-Behnken central combination test was carried out to investigate the effects of each test factor on the evaluation indexes and to determine the optimal parameter combination. According to the pre-test, it was found that the seeding performance was good when the suction hole diameter, forward speed and negative pressure were set to 2.7~3.5 mm, 1.67~3.33 m/s (6.0~12.0 km/h), and 2000~4000 Pa, respectively. Therefore, the levels of each test factor were selected as shown in Table 3. A total of 17 test groups were conducted, with each group repeated 3 times, and the average value was taken as the final evaluation index.

Table 3

The levels of test factors for Box-Behnken test

Levels	Test factors		
	Suction hole diameter X_1 / (mm)	Forward speed X_2 / (m/s)	Negative pressure X_3 / (Pa)
-1	2.7	1.67	2000
0	3.1	2.5	3000
1	3.5	3.33	4000

(2) Based on the optimal parameter combination obtained from the above tests, four levels of 1.67, 2.22, 2.78 and 3.33 m/s (6, 8, 10 and 12 km/h) were selected to carry out the high-speed adaptability test of the seed-metering device with forward speed as the test factor. Each group of tests was repeated 3 times, and the average of the results was taken as the final evaluation index.

RESULTS AND DISCUSSION

Validation of the airflow field model

The pressure registered values at the suction hole endface in both physical and simulation tests are shown in Fig. 8.

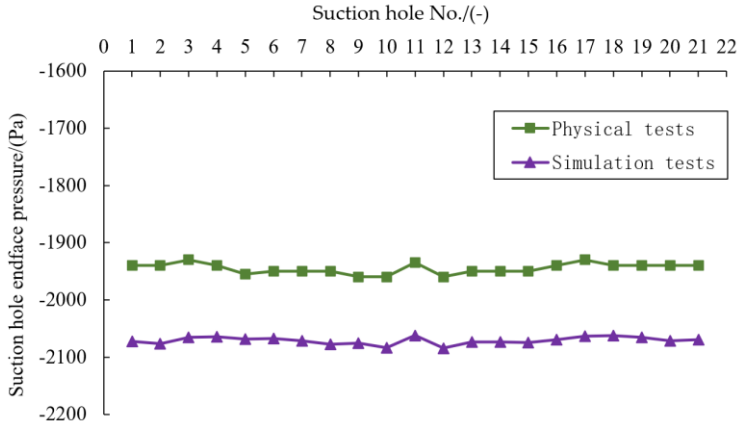

Fig. 8 – Pressure values at the suction hole endface in both physical and simulation tests

Note: 1. Simulation settings: Outlet −3000 Pa, Inlet(s) 0 Pa, dynamic zone rotation speed 0 r/min, residual convergence 10^{-4}, time step 0.003571429 s, 500 steps.
2. Test repeats for 3 times.

As can be seen from Fig. 8, the absolute values of the pressure at the suction hole endface in the physical tests were lower than the simulation values, which was mainly due to the airflow loss caused by the gap between the seeding plate and back shell. Since the seeding plate and the back shell were in axial linear contact, considering the difficulty of ensuring coaxiality due to the limited precision of 3D printing, a clearance of 0.6 mm was reserved between the back shell and the seeding plate to allow the seeding plate smooth rotation. Therefore, the absolute pressure values measured in the physical tests were all lower than those obtained from the simulation tests, but the relative errors between them were all less than 7.04%, indicating that the airflow field model was suitable for the subsequent simulation analysis of the seed-metering device.

Simulation analysis results

CFD simulation results *for the negative pressure air chamber*

Effect of Air Outlet Hole Angle and Position on the Suction Hole Endface Pressure

The design and results of the orthogonal test on the air outlet hole angle and position of the negative pressure air chamber are shown in Table 4, and the results of extreme difference analysis are shown in Table 5. As shown in the table, the factors influencing the pressure average at the suction hole endface in the seed filling area ranked in the following order: front and rear inclination angle θ_c, up and down inclination angle θ_b and position angle θ_a, and for this evaluation index, the optimal combination was $\theta_{c_2}\theta_{b_2}\theta_{a_1}$. The factors influencing the pressure standard deviation at the suction hole endface in the seed cleaning and carrying areas ranked in the following order: position angle θ_a, front and rear inclination angle θ_c and up and down inclination angle θ_b, and for this evaluation index, the optimal combination was $\theta_{a_2}\theta_{c_2}\theta_{b_2}$. Therefore, it can be concluded that the up and down inclination angle should be set to level θ_{b_2}, and the front and rear inclination angle should be set to level θ_{c_2}. However, the optimal value for the position angle remains uncertain and requires further determination through analysis of variance.

Table 4

Orthogonal test design and results

Test serial number	Test factors			Evaluation indexes	
	θ_a	θ_b	θ_c	Pressure average at the suction hole endface in the seed filling area Y_1/(Pa)	Pressure standard deviation at the suction hole endface in the seed cleaning and carrying areas Y_2/(Pa)
1	1	1	1	1207.69	81.11
2	1	2	2	1354.77	70.72
3	1	3	3	1077.77	90.99
4	2	2	3	1145.55	30.06
5	2	3	1	1206.23	31.07
6	2	1	2	1164.85	29.31
7	3	3	2	1190.64	101.31
8	3	1	3	1055.01	113.00
9	3	2	1	1275.71	91.20

Note: 1. Simulation settings: Outlet −3000 Pa, Inlet(s) 0 Pa, dynamic zone rotation speed 30 r/min, time step 0.003571429 s, 570 steps. 2. Test repeats for 3 times.

Table 5

Extreme difference analysis of orthogonal test results

Evaluation indexes	Test factors	Factor levels averages			Maximum difference/(Pa)	Optimal parameter combination
		Level 1/(Pa)	Level 2/(Pa)	Level 3/(Pa)		
Pressure average at the suction hole endface in the seed filling area Y_1/(Pa)	θ_a	1213.41	1172.21	1173.79	41.20	$\theta_{c_2}\theta_{b_2}\theta_{a_1}$
	θ_b	1142.52	1258.68	1158.21	116.16	
	θ_c	1229.88	1236.75	1092.78	143.97	
Pressure standard deviation at the suction hole endface in the seed cleaning and carrying areas Y_2/(Pa)	θ_a	80.94	30.15	101.84	71.69	$\theta_{a_2}\theta_{c_2}\theta_{b_2}$
	θ_b	74.47	63.99	74.46	10.48	
	θ_c	67.79	67.11	78.02	10.91	

Note: 1. Simulation settings: Outlet −3000 Pa, Inlet(s) 0 Pa, dynamic zone rotation speed 30 r/min, time step 0.003571429 s, 570 steps. 2. Test repeats for 3 times.

The results of variance analysis are shown in Table 6. As can be seen from the table, for the pressure average at the suction hole endface in the seed filling area, the front and rear inclination angle had a significant effect on it, and the remaining two factors have no significant effect. For the pressure standard deviation at the suction hole endface in the seed cleaning and carrying areas, all the test factors had a highly significant effect, which was consistent with the results of the extreme difference analysis. Among the three test factors, the position angle had no significant effect on the pressure average at the suction hole endface in the seed filling area, with a contribution rate of 4.78%. However, it had a highly significant effect on the pressure standard deviation at the suction hole endface in the seed cleaning and carrying areas, with a contribution rate as high as 94.83%. Therefore, the selection of the position angle should be primarily based on the pressure standard deviation. Combined with the results of the extreme difference analysis, the optimal level for the air outlet position angle was determined to be θ_{a_2}. Since the factor combination $\theta_{a_2}\theta_{b_2}\theta_{c_2}$ was not included in the orthogonal test design, a simulation verification test was conducted for the airflow field model under this combination using the same method. After the simulation, statistical analysis showed that the pressure average at the suction hole endface in the seed filling area was 1257.64 Pa, which was lower than that of groups 2 and 9 in the orthogonal test, with a maximum pressure difference of 97.13 Pa. The pressure standard deviation at the suction hole endface in the seed cleaning and carrying areas was 8.92 Pa, which was lower than all standard deviations in the orthogonal test. This indicated that when the air outlet was located in the central plane of the negative pressure air chamber, the pressure at the suction hole endface in the seed filling area was not the highest, but the pressure variation in the seed cleaning and seed carrying areas was minimized, resulting in the most stable cotton seed adsorption. Since increasing pressure at the suction hole endface in the seed filling area can be achieved by adjusting the air outlet negative pressure, while reducing the pressure standard deviation at the suction hole endface in the seed cleaning and carrying areas was difficult to accomplish through changing external parameters, the optimal combination of air outlet angle and position was determined to be $\theta_{a_2}\theta_{b_2}\theta_{c_2}$, namely, the position angle of 135°, up and down inclination angle of 0°, front and rear inclination angle of 0°.

Table 6

Variance analysis of orthogonal test results

Source of variation	Pressure average at the suction hole endface in the seed filling area				Pressure standard deviation at the suction hole endface in the seed cleaning and carrying areas			
	Sum of squares	Degree of freedom	*F*-value	Contribution /(%)	Sum of squares	Degree of freedom	*F*-value	Contribution /(%)
θ_a	3269.93	2	1.91	4.78	8156.42	2	4301.73**	94.83
θ_b	23832.41	2	13.93	34.85	219.28	2	115.65**	2.55
θ_c	39572.98	2	23.13*	57.87	223.89	2	118.08**	2.60
Error	1710.77	2		2.50	1.90	2		0.02
Cor total	68386.09	8			8601.49	8		

*Note: 1. Simulation settings: Outlet −3000 Pa, Inlet(s) 0 Pa, dynamic zone rotation speed 30 r/min, time step 0.003571429 s, 570 steps; 2. Test repeats for 3 times; 3. * represents the factor with a significant influence on the index, ** represents factor with a highly significant influence on the index.*

Effect of Negative Pressure Air Chamber Width and Thickness on the Suction Hole Endface Pressure

The results of the two-factor test on the negative pressure air chamber width and thickness are shown in Table 7. As observed, with the increase of thickness, the pressure average at the suction hole endface in the seed filling area gradually increased, while the pressure standard deviation at the suction hole endface in the seed cleaning and carrying areas gradually decreased. This was primarily because an increase in thickness enlarged the airflow circulation area within the air chamber. According to fundamental fluid dynamics theory, a smaller airflow circulation area results in greater resistance losses. Therefore, increasing the thickness of the negative pressure air chamber was conducive to reducing airflow losses and promoting the uniform distribution of suction hole endface pressure. As the width increased, the trend of the average pressure at the suction hole endface in the seed-filling area was not obvious, with only small differences observed, while the pressure standard deviation at the suction hole endface in the seed-cleaning and seed-carrying areas gradually decreased. The main reason is that the suction holes are located along the width of the air chamber, and their diameter is much smaller than the chamber width. Thus, airflow in this direction remained smooth. Consequently, width changes had little effect on the average pressure at the suction hole endface in the seed-filling area, whereas the increased circulation area promoted a more uniform pressure distribution. The results of variance analysis are shown in Table 8.

As can be seen from the table, thickness had a greater influence than width on both the pressure average at the suction hole endface in the seed filling area and the standard deviation in the seed cleaning and carrying areas, which was consistent with the above analysis. In order to obtain a higher pressure average at the suction hole endface in the seed filling area and a lower pressure standard deviation at the suction hole endface in the seed cleaning and carrying areas, the width and thickness of the negative pressure air chamber were selected as 30 mm and 20 mm, respectively.

Table 7

Two-factor test results

Thickness c_0/(mm) / Width b_0/(mm)	Pressure average at the suction hole endface in the seed filling area Y_1/(Pa)			Pressure standard deviation at the suction hole endface in the seed cleaning and carrying areas Y_2/(Pa)		
	12	16	20	12	16	20
22	1229.35	1248.70	1254.92	52.02	22.48	21.16
26	1233.53	1249.32	1257.01	25.22	11.13	10.93
30	1238.97	1246.61	1257.64	23.78	10.65	8.92

Note: 1. Simulation settings: Outlet −3000 Pa, Inlet(s) 0 Pa, dynamic zone rotation speed 30 r/min, time step 0.003571429 s, 570 steps; 2. Test repeats for 3 times.

Table 8

Variance analysis of two-factor test results

Source of variation	Pressure average at the suction hole endface in the seed filling area				Pressure standard deviation at the suction hole endface in the seed cleaning and carrying areas			
	Sum of squares	Degree of freedom	*F*-value	Contribution /(%)	Sum of squares	Degree of freedom	*F*-value	Contribution /(%)
b_0	18.20	2	1.00	2.18	565.82	2	9.76*	39.26
c_0	782.01	2	42.94**	93.47	759.27	2	13.10*	52.69
Error	36.43	4		4.35	115.96	4		8.05
Cor Total	836.64	8			1441.05	8		

Note: 1. Simulation settings: Outlet −3000 Pa, Inlet(s) 0 Pa, dynamic zone rotation speed 30 r/min, time step 0.003571429 s, 570 steps; 2. Test repeats for 3 times.

DEM-CFD coupling simulation results for the seed throwing link

The single cotton seed throwing process is shown in Fig. 9. As illustrated in the figure, when the positive pressure of the seed throwing air nozzle was 1500 Pa, the cotton seed at the suction hole endface was blown into the collection hole under the drag force of the seed throwing air nozzle. At 1.581 s, the seed makes its first contact and collision with the inner wall of the back shell, and was subsequently bounced upward, followed by a second and third collision with the inner wall at 1.695 s and 1.752 s, respectively. After that, the seed no longer exhibited obvious bouncing behavior but instead moved along the inner wall until it was discharged at the seed-throwing port. This simulation phenomenon indicated that, after entering the collection hole, the cotton seed underwent multiple contacts and collisions with the inner wall of the back shell. Therefore, the starting position angle of the seed-throwing port should be set slightly backward to avoid degraded seeding performance caused by seed bouncing.

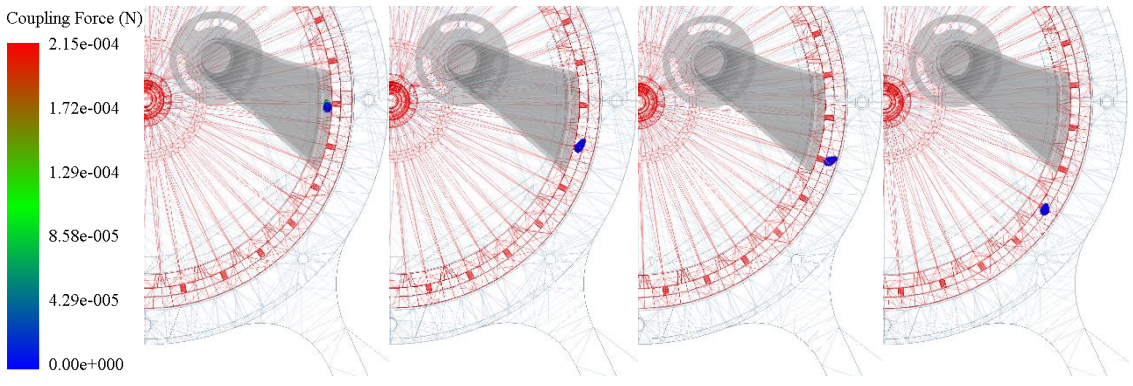

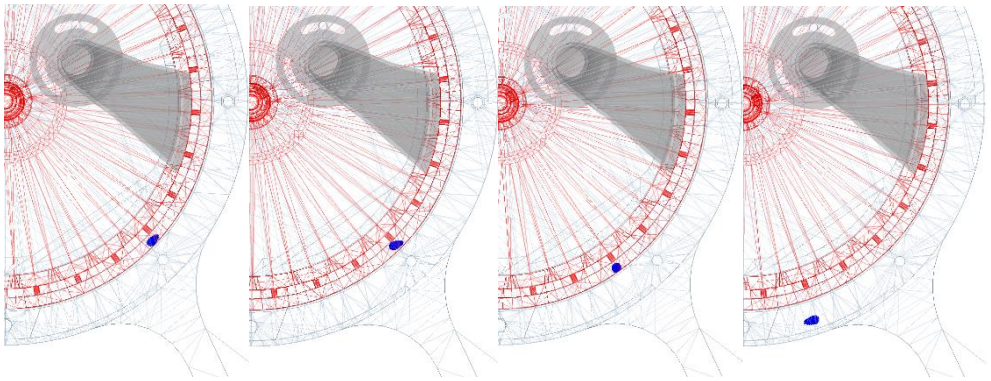

(e) (f) (g) (h)

Fig. 9 - Seed throwing process for single cotton seed

(a) 1.506 s, (b) 1.566 s, (c) 1.581 s, (d) 1.656 s, (e) 1.695 s, (f) 1.707 s, (g) 1.752 s, (h) 1.830 s

Note: 1. Simulation settings: Freestream model, Outlet −3000 Pa, Inlet_1 0 Pa, Inlet_2 0 Pa, Inlet_3 1500 Pa, dynamic zone rotation speed 35.71 r/min, solid time step 3×10^{-7} s, fluid time step 3×10^{-5} s, 100000 steps; 2. Test repeats for 10 times.

The DEM–CFD coupling simulation results for the seed-throwing process are presented in Table 9. As shown, when the seed-throwing pressure was 500 Pa, the outlet velocity of the seed-throwing air nozzle was 19.54 m/s, which was insufficient to blow the cotton seed into the collection hole. When the pressure was ≥1000 Pa, seeds were blown smoothly into the collection hole, and with increasing pressure, the nozzle outlet airflow rate also increased, accelerating seed entry. Consequently, the initial contact angle increased gradually, while the stable contact angles were consistently ≥37.23°, although no clear variation pattern was observed. Simulation and post-processing analyses further revealed no obvious regularity in the bouncing behavior of seeds within the collection hole. Based on this analysis, the seed-throwing pressure should be no less than 1000 Pa to ensure smooth seed delivery. However, considering the gap between the seeding plate and the back shell during actual operation, residual adsorption forces may still act on the seeds at the suction-hole end face after leaving the negative-pressure air chamber. Therefore, the seed-throwing pressure should be appropriately increased, and in this study, a value of 1500 Pa was selected. In addition, to minimize the bouncing of seeds in the collection hole and avoid adverse effects on seeding performance, the starting position angle of the seed-throwing port should be smaller than the minimum stable contact angle of the seeds (37.23°). Accordingly, an angle of 30° was adopted.

Table 9

Simulation test results of seed throwing link

Seed throwing pressure/(Pa)	Outlet velocity of seed throwing air nozzle/(m/s)	Initial contact angle / (°)	Initial contact angle minimum / (°)	Stable contact angle /(°)	Stable contact angle minimum / (°)
500	19.54				
1000	27.85	69.23±1.82	67.1	41.03±1.95	38.03
1500	34.29	75.37±1.43	72.18	39.87±1.46	37.23
2000	39.65	77.84±1.56	75.17	40.26±1.52	37.77

Note: 1. Simulation settings: Freestream model, Outlet −3000 Pa, Inlet_1 0 Pa, Inlet_2 0 Pa, Inlet_3 1500 Pa, dynamic zone rotation speed 35.71 r/min, solid time step 3×10^{-7} s, fluid time step 3×10^{-5} s, 100000 steps; 2. Test repeats for 10 times.

Seeding performance test results of the seed-metering device

Box-Behnken Test

The protocol and results of the Box-Behnken test are shown in Table 10.

Table 10

Box-Behnken test protocol and results

Test serial number	Test factors			Evaluation indexes		
	X_1	X_2	X_3	Qualification index A_1/(%)	Multiple sowing index D_1/(%)	Missed sowing index M_1/(%)
1	-1	-1	0	90.25	3.32	6.43
2	-1	0	-1	81.38	1.06	17.56
3	-1	0	1	91.36	2.78	5.86
4	-1	1	0	88.64	3.69	7.67
5	0	-1	-1	86.78	2.69	10.53
6	0	-1	1	89.46	6.15	4.39

Test serial number	Test factors			Evaluation indexes		
	X_1	X_2	X_3	Qualification index A_1/(%)	Multiple sowing index D_1/(%)	Missed sowing index M_1/(%)
7	0	0	0	97.19	1.19	1.62
8	0	0	0	96.54	1.85	1.61
9	0	0	0	95.93	1.59	2.48
10	0	0	0	94.26	2.53	3.21
11	0	0	0	96.88	1.70	1.42
12	0	1	-1	77.00	4.43	18.57
13	0	1	1	86.98	6.29	6.73
14	1	-1	0	91.13	5.65	3.22
15	1	0	-1	86.92	2.74	10.34
16	1	0	1	88.93	8.52	2.55
17	1	1	0	88.17	6.18	5.65

Note: 1. Air outlet hole position angle 135°, up and down inclination angle 0° and front and rear inclination angle 0°; air chamber thickness 20 mm and width 30 mm; seed throwing pressure 1500 Pa, seed throwing port starting position angle 30°; 2. Test repeats for 3 times.

In order to further analyze the significance of the effect of each test factor and its interaction on the evaluation indexes, Design-Expert 10.0.4 was used to carry out a multiple regression analysis on the test results and establish a quadratic regression model between the test factors and evaluation indexes. The significance analysis results are shown in Table 11. As can be seen from the table, the regression models were all highly significant (P≤0.01) and the lack of fit were all insignificant (P>0.05), so the regression equations were well fitted to the test data. For the qualification index, the linear terms X_2, X_3 and quadratic term X_2^2, X_3^2 had a highly significant effect on it (P≤0.01), interaction term X_1X_3, X_2X_3 and quadratic term X_1^2 had a significant effect on it (0.01<P≤0.05), and the remaining terms had no significant effect on it (P>0.05). For the multiple sowing index, the linear terms X_1, X_3 and quadratic term X_2^2, X_3^2 had a highly significant effect on it (P≤0.01), interaction term X_1X_3 and quadratic term X_1^2 had a significant effect on it (0.01<P≤0.05), and the remaining terms had no significant effect on it (P>0.05). For the missed sowing index, all the linear terms and quadratic term X_2^2, X_3^2 had a highly significant effect on it (P≤0.01) and the remaining terms had no significant effect on it (P>0.05). Moreover, the order of test factors affecting the qualification index was: negative pressure>forward speed>suction hole diameter. And the order of test factors affecting the multiple sowing index and missed sowing index was: negative pressure>suction hole diameter>forward speed. The quadratic regression equations between the test factors and evaluation indexes are as follows:

$$A_1 = 96.16 + 0.44X_1 - 2.10X_2 + 3.08X_3 - 0.34X_1X_2 - 1.99X_1X_3 + 1.83X_2X_3 - 2.26X_1^2 - 4.35X_2^2 - 6.75X_3^2 \quad (3)$$

$$D_1 = 1.77 + 1.53X_1 + 0.35X_2 + 1.6X_3 + 0.04X_1X_2 + 1.01X_1X_3 - 0.4X_2X_3 + 0.91X_1^2 + 2.03X_2^2 + 1.09X_3^2 \quad (4)$$

$$M_1 = 2.07 - 1.97X_1 + 1.76X_2 - 4.68X_3 + 0.3X_1X_2 + 0.98X_1X_3 - 1.42X_2X_3 + 1.35X_1^2 + 2.33X_2^2 + 5.66X_3^2 \quad (5)$$

where:

X_1, X_2 and X_3 represent the coded levels (−1, 0, +1), and the coding of actual factor levels is shown in Table 3.

Table 11

Variance analysis of Box-Behnken test results

Source of variation	Qualification index			Multiple sowing index			Missed sowing index		
	Sum of squares	F-value	P-value	Sum of squares	F-value	P-value	Sum of squares	F-value	P-value
Model	463.19	26.21	0.0001**	73.34	22.66	0.0002**	421.13	27.93	0.0001**
X_1	1.55	0.79	0.4040	18.73	52.09	0.0002**	31.05	18.53	0.0035**
X_2	35.41	18.03	0.0038**	0.97	2.69	0.1452	24.68	14.73	0.0064**
X_3	75.95	38.68	0.0004**	20.54	57.14	0.0001**	175.50	104.74	<0.0001**
X_1X_2	0.46	0.23	0.6447	0.01	0.018	0.8976	0.35	0.21	0.6597
X_1X_3	15.88	8.09	0.0249*	4.12	11.46	0.0117*	3.82	2.28	0.1747
X_2X_3	13.32	6.78	0.0352*	0.64	1.78	0.2239	8.12	4.85	0.0636
X_1^2	21.51	10.95	0.0130*	3.50	9.73	0.0169*	7.66	4.57	0.0699
X_2^2	79.77	40.62	0.0004**	17.29	48.09	0.0002**	22.78	13.60	0.0078**
X_3^2	191.98	97.77	<0.0001**	5.02	13.95	0.0073**	134.93	80.53	<0.0001**
Residual	13.75			2.52			11.73		

Source of variation	Qualification index			Multiple sowing index			Missed sowing index		
	Sum of squares	*F*-value	*P*-value	Sum of squares	*F*-value	*P*-value	Sum of squares	*F*-value	*P*-value
Lack of Fit	8.36	2.07	0.2470	1.56	2.17	0.2341	9.42	5.45	0.0674
Pure Error	5.39			0.96			2.31		
Cor Total	476.93			75.86			432.86		

*Note: 1. Air outlet hole position angle 135°, up and down inclination angle 0° and front and rear inclination angle 0°; air chamber thickness 20 mm and width 30 mm; seed throwing pressure 1500 Pa, seed throwing port starting position angle 30°; 2. Test repeats for 3 times; 3. P ≤ 0.01 (Highly significant, **); 0.01 < P ≤ 0.05 (Significant, *).*

So as to obtain the best combination of test factors, taking the maximum qualification index and the minimum multiple and missed sowing index as the final optimization objective, combined with the boundary conditions of each test factor, the established quadratic regression models were solved by multi-factor optimization.

The objective functions and constraints are as follows:

$$\begin{cases} \max A_1(x_1, x_2, x_3) \\ \min D_1(x_1, x_2, x_3) \\ \min M_1(x_1, x_2, x_3) \\ s.t. \begin{cases} 2.7\ mm \le x_1 \le 3.5\ mm \\ 1.67\ m/s \le x_2 \le 3.33\ m/s \\ 2000\ Pa \le x_3 \le 4000\ Pa \end{cases} \end{cases} \quad (6)$$

Using the optimization module of Design-Expert 10.0.4, the best combination of parameters was determined to be: suction hole diameter of 3.1 mm, forward speed of 2.33 m/s (8.4 km/h), and negative pressure of 3178 Pa. Under these conditions, the seeding performance was optimal, with a qualification index of 96.67%, multiple sowing index of 2.04%, and missed sowing index of 1.29%. To verify the reliability of the optimized parameters, the seeding performance test of seed-metering device was conducted for three repetitions. The average values of the evaluation indexes were as follows: qualification index of 96.25%, multiple sowing index of 1.83%, and missed sowing index of 1.92%, which were generally consistent with the predicted values from the software.

High-speed Adaptability Test

The high-speed adaptability test results of the inside-filling pneumatic cotton high-speed precision seed-metering device are shown in Table 12. As shown in the table, with increasing forward speed, the qualification index first increased and then decreased, the multiple sowing index first decreased and then increased, while the missed sowing index gradually increased, which was consistent with the previous analysis. When the forward speed ranged from 1.67 to 3.33 m/s (6–12 km/h), the qualification index exceeded 91%, and both the multiple sowing index and the missed sowing index remained below 5%. These values were superior to the agronomic requirements specified in JB/T 10293-2013 'Specifications for Single Seed Drills (Precision Drills),' which require a qualification index ≥75%, a multiple sowing index ≤20%, and a missed sowing index ≤10%. This indicates that the optimized seed-metering device meets the high-speed sowing requirements for cotton.

Table 12

High-speed adaptability test results

Forward speed/(m/s)	Qualification index/(%)	Multiple sowing index/(%)	Missed sowing index/(%)
1.67	94.34	3.98	1.68
2.22	95.66	2.61	1.73
2.33	96.25	1.83	1.92
2.78	94.81	2.75	2.44
3.33	91.43	4.55	4.02

Note: 1. Air outlet hole position angle 135°, up and down inclination angle 0° and front and rear inclination angle 0°; air chamber thickness 20 mm and width 30 mm; seed throwing pressure 1500 Pa, seed throwing port starting position angle 30°; 2. Test repeats for 3 times.

CONCLUSIONS

(1) The CFD simulation results of the negative-pressure air chamber showed that, in the orthogonal test of air outlet hole angle and position, the order of influence on the average pressure at the suction hole end face in the seed-filling area was: front–rear inclination angle > vertical inclination angle > position angle. For the pressure standard deviation in the seed-cleaning and seed-carrying areas, the order was: position angle > front–rear inclination angle > vertical inclination angle. The optimal parameter combination was a position angle of 135°, a vertical inclination angle of 0°, and a front–rear inclination angle of 0°. In the two-factor test of chamber thickness and width, thickness had a greater effect than width on both the average pressure in the seed-filling area and the standard deviation in the seed-cleaning and seed-carrying areas, with the optimal combination being a thickness of 20 mm and a width of 30 mm.

(2) The DEM–CFD simulation results of the seed-throwing process showed that, after falling into the collection hole, cotton seeds underwent multiple collisions with the inner wall of the back shell before moving along it. At a seed-throwing pressure of 1500 Pa, the seeds could be smoothly blown into the collection hole. Setting the starting position angle of the seed-throwing port to 30° reduced the adverse effects of seed bouncing within the collection hole on the seed-throwing performance.

(3) The results of the Box–Behnken test indicated that the factors influencing the qualification index ranked in the following order: negative pressure > forward speed > suction hole diameter. For the multiple sowing index and missed sowing index, the order was: negative pressure > suction hole diameter > forward speed. The optimal parameter combination was a suction hole diameter of 3.1 mm, a forward speed of 2.33 m/s (8.4 km/h), and a negative pressure of 3178 Pa. Bench tests verified the corresponding evaluation indexes, yielding a qualification index of 96.25%, a multiple sowing index of 1.83%, and a missed sowing index of 1.92%.

(4) The results of the high-speed adaptability test showed that, as forward speed increased, the qualification index first increased and then decreased, the multiple sowing index first decreased and then increased, and the missed sowing index gradually increased. When the forward speed was 1.67–3.33 m/s (6–12 km/h), the qualification index remained above 91%, while both the multiple and missed sowing indices were below 5%, thereby meeting the agronomic requirements for high-speed precision cotton seeding.

ACKNOWLEDGEMENT

This study was supported by the Research Funding of Wuhan Polytechnic University (2024RZ081; XQ2025006) and Double First Class School Funding - Discipline Building (01003009).

REFERENCES

[1] Bie, S. & Zhang, J.H. (2018). Cotton green light and simple efficient cultivation technology. 1rd ed., *Hubei Science and Technology Press*, Wuhan, China, pp. 1-2.

[2] Bustos-Gaytán, A., Saldaña-Robles, N., Joya-Cárdenas, D.R., Gutiérrez-Vaca, C., Alfaro-Ayala, J.A., Barco-Burgos, J., & Saldaña-Robles, A. (2025). Advancements in pneumatic seed-metering devices: A review of numerical and experimental approaches. *Results in Engineering*, *26*, 105626. https://doi.org/10.1016/j.rineng.2025.105626

[3] Cao, X.Y., Wang, L., Liao, Q.X., & Liao, Y.T. (2024). Simulation of the mixing component of a horizontal air-assisted centralised wheat metering device. *Biosystems Engineering*, *243*, 13-26. https://doi.org/10.1016/j.biosystemseng.2024.05.002

[4] Cortez, J.W., Anghinoni, M., & Arcoverde, S.N. (2020). Seed metering mechanisms and tractor-seeder forward speed on corn agronomic components. *Engenharia Agrícola*, *40(1)*, 61-68. https://doi.org/10.1590/1809-4430-Eng.Agric.v40n1p61-68/2020

[5] Dong, J., Wu, J., Zhu, Y., & Gao, X. (2025). Investigation on Seed-Filling Effect of Quantitative Precision Filling High-Speed Seed-Metering Device for Maize. *Agriculture*, *15*(14), 1517. https://doi.org/10.3390/agriculture15141517

[6] Gao, X.J., Yu, L.Y., Wu, X.P., Huang, Y.X., & Yan, X.L. (2023). Design and Experiment of Intelligent Seed Supply System of Air-assisted High Speed Precision Maize Seed Metering Device. *Transactions of the Chinese Society for Agricultural Machinery*, *54*(s1), 66-75. https://doi.org/10.6041/j.issn.1000-1298.2023.S1.008

[7] Guzman, L. (2024). *Simulation of Agricultural Air Seeding Systems Using the Discrete Element Method and Computational Fluid Dynamics* [Doctoral dissertation, University of Manitoba]. University of Manitoba's Institutional Repository. http://hdl.handle.net/1993/38061

[8] Guzman, L., Chen, Y., & Landry, H. (2020). Coupled CFD-DEM Simulation of Seed Flow in an Air Seeder Distributor Tube. *Processes*, *8(12)*, 1597. https://doi.org/10.3390/pr8121597

[9] Hu, M.J., Xia, J.F., Zhou, Y., Luo, C.M., Zhou, M.K., & Liu, Z.Y. (2022). Measurement and Calibration of the Discrete Element Parameters of Coated Delinted Cotton Seeds. *Agriculture*, *12*(2), 286. https://doi.org/10.3390/agriculture12020286

[10] Hussain, S., Chen, Y., Yu, X., Farid, M.U., Ghafoor, A., Alshamali, S.J., Munir, T., & Hu, J. (2025). Design Optimization and Aerodynamic Investigations of Air Suction Seed Metering Systems through CFD-DEM Approach. *Smart Agricultural Technology*, *12*, 101082. https://doi.org/10.1016/j.atech.2025.101082

[11] Li, C., Zhang, D.X., Yang, L., Cui, T., He, X.T., Zhang, K.L., Li, Z.M., Li, H.S., Xing, S.L., Dong, J.Q., Jiang, Y.Y., Zhang, X.S., Wu W., & Zhang, C.K. (2025). Design of a streamlined structure to minimize seed damage in high-speed centrifugal seed metering devices. *Powder Technology*, *464*, 121251. https://doi.org/10.1016/j.powtec.2025.121251

[12] Li, M.S., Wang, P., Yan, Y.L., Xie, S.Y., Liu, Z.J., Liu, F.Y., & Chen, X.Z. (2025). Design and experiment of chain-spoon type maize precision seed metering device. *Transactions of the Chinese Society of Agricultural Engineering*, 447-459.

[13] Li, Y.H., Yang, L., Zhang, D.X., Cui, T., Zhang, K.L., Xie, C.J., & Yang, R.M. (2020). Analysis and test of linear seeding process of maize high speed precision metering device with air suction. *Transactions of the Chinese Society of Agricultural Engineering*, *36*(9), 26-35. https://doi.org/10.11975/j.issn.1002-6819.2020.09.003

[14] Li, Y.H., Zhao, S., Yang, L., Song, Q., Li, B.G., & Yang, F.Z. (2024). Design and Test of High-speed Precision Seeder of Independent Fractionated Soybean Double-row Brush. *Transactions of the Chinese Society for Agricultural Machinery*, *55*(06), 101-110. https://doi.org/10.6041/j.issn.1000-1298.2024.06.010

[15] Li, Z.D., He, S., Zhong, J.Y., Han, J.F., Chen, Y.X., & Song, Y. (2021). Parameter optimization and experiment of the disturbance pneumatic plate hole metering device for rapeseed. *Transactions of the Chinese Society of Agricultural Engineering*, *37*(17), 1-11. https://doi.org/10.11975/j.issn.1002-6819.2021.17.001

[16] Liu, Z.Y., Xia, J.F., Hu, M.J., Du, J., Luo, C.M., & Zheng, K. (2021). Design and analysis of a performance monitoring system for a seed metering device based on pulse width recognition. *Plos one*, *16*(12), e0261593. https://doi.org/10.1371/journal.pone.0261593

[17] Pareek, C.M., Tewari, V.K., & Machavaram R. (2023). Multi-objective optimization of seeding performance of a pneumatic precision seed metering device using integrated ANN-MOPSO approach. *Engineering Applications of Artificial Intelligence*, *117*, 105559. https://doi.org/10.1016/j.engappai.2022.105559

[18] Sun, W.S., Yi, S.J., Qi, H.L., Li, Y.F., Dai, Z.B., Zhang, Y.P., Yuan, J.S. & Wang, S. (2025). Design and optimization of air-assisted spiral seed-supply device for high-speed dense planting maize seeder. *INMATEH - Agricultural Engineering*, *75*(1), 13-25. https://doi.org/10.35633/inmateh-75-01

[19] Wan, L., Wang, H.C., Che, G., Sun, W.S., & Chen, Z.F. (2022). Design and performance test of spoiler blades of the direct seed-metering device for rice. *INMATEH - Agricultural Engineering*, *68*(3), 60-70. https://doi.org/10.35633/inmateh-68-06

[20] Wang, W.W., Song, L.Z., An, X., Quan, L.Z., Xie, D.B., Chen, Y.X., Li, Z.D., Wu, Z.C., & Chen, L.Q. (2025). Optimizing seed filling performance of the double-filling air suction maize and soybean seed metering device based on DEM-CFD coupling method. *Computers and Electronics in Agriculture*, *237*, 110586. https://doi.org/10.1016/j.compag.2025.110586

[21] Xu, G.J. (2018). *Design and experiment of pneumatic cylinder array precision seed-metering device for cotton*. [Master dissertation, Shihezi University]. Shihezi University Campus Repository.

[22] Yang, L., Li, Z.M., Zhang, D.X., Li, C., Cui, T., & He, X.T. (2024). Design and test of the T-shaped hole of centrifugal high-speed maize precision seed metering device. *Transactions of the Chinese Society of Agricultural Engineering*, *40*(07), 50-60. https://doi.org/10.11975/j.issn.1002-6819.202312208

[23] Yatskul, A., & Lemiere, J.P. (2018). Establishing the conveying parameters required for the air-seeders. *Biosystems Engineering*, *166*, 1-12. https://doi.org/10.1016/j.biosystemseng.2017.11.001

[24] Zang, Y, Huang, Z.S., Qin, W., He, S.Y., Qian, C., Jiang, Y.C., Tao, W.Y., Zhang, M.L., & Wang, Z.M. (2024). Design of hybrid rice air-suction single-seed metering device. *Transactions of the Chinese*

Society of Agricultural Engineering, *40*(6), 181-191. https://doi.org/10.11975/j.issn.1002-6819.202310212

[25] Zha, X.T., Chen, L., Chen, D.Q., He, Y.P., & Yang, R.B. (2024). Design and Testing of a Branched Air-Chamber Type Pneumatic Seed Metering Device for Rice. *Agriculture*, *14*(11), 1934. https://doi.org/10.3390/agriculture14111934

[26] Zhang, C.Y., Kang, J.M., Peng, Q.J., Zhang, N.N., Wang, X.Y., & Jian, S.C. (2021). Design and Test of Secondary Seed Feeding Mechanism of Air-suction Roller Dibbler for Cotton. *Transactions of the Chinese Society for Agricultural Machinery*, *52*(6), 106-116. https://doi.org/10.6041/j.issn.1000-1298.2021.06.011

[27] Zhang, X.J., Zhang, H.T., Shi, Z.L., Jin, W., Chen, Y., & Yu, Y.L. (2022). Design and experiments of seed pickup status monitoring system for cotton precision dibblers. *Transactions of the Chinese Society of Agricultural Engineering*, *38*(5), 9-19. https://doi.org/10.11975/j.issn.1002-6819.2022.05.002

[28] Zhao, P.F., Gao, X.J., Su, Y., Xu, Y., & Huang, Y.X. (2024). Investigation of Seeding Performance of a Novel High-speed Precision Seed Metering Device Based on Numerical Simulation and High-speed Camera. *Computers and Electronics in Agriculture*, *217*, 108563. https://doi.org/10.1016/j.compag.2023.108563

[29] Zhou, H.J., Zhang, C.L., Liu, T., Wang, Y.Z., Fang, J., & Hu, A.T. (2024). Design and experiment of annular air-blowing assisted seed guiding device for corn no-till seeder. *INMATEH - Agricultural Engineering*, *73*(2),50-62. https://doi.org/10.35633/inmateh-73-04